A new formula based on computational fluid dynamics for estimating maximum depth of scour by jets from overflow dams

Sherong Zhang, Bohui Pang and Gaohui Wang

ABSTRACT

The prediction of the maximum depth of the scour hole formed downstream of overflow dams is critical in determining the safety of hydraulic structures. Most of the conventional formulae are not able to consider complex hydraulic and morphologic conditions. A new formula for estimating the maximum depth of the scour hole based on computational fluid dynamics (CFD), which can be used to simulate the complicated phenomenon, is proposed. The relationship between the maximum velocity in numerical simulations and the maximum scour depth is reflected in this formula, which is established using the Levenberg–Marquardt (LM) algorithm. The validity of this proposed formula is discussed by comparing this formula with three other conventional formulae. The prediction formula based on CFD is applied to the Wuqiangxi Dam, and the absolute deviation of the predicted maximum scour depth (35.44 m) from the measured depth (36.00 m) is 0.56 m.

Key words | computational fluid dynamics (CFD), Levenberg–Marquardt (LM) algorithm, maximum scour depth, prediction formula, rock bed

Sherong Zhang
Bohui Pang (corresponding author)
Gaohui Wang
State Key Laboratory of Hydraulic Engineering Simulation and Safety,
Tianjin University,
Tianjin 300072,
China
E-mail: *tjudam@126.com*

NOTATION

a	coefficient in the power-law function relationship
A_x	fractional areas open to flow in x directions
A_y	fractional areas open to flow in y directions
A_z	fractional areas open to flow in z directions
b	exponential in the power-law function relationship
B	channel width
b_g	sluice gate opening
b_j	jet width
b_w	weir width
c	exponential in the power-law function relationship
C	air reduction coefficient
C_{sp}	shear production coefficient
$C_{\varepsilon 1}$	1.42
$C_{\varepsilon 2}$	non-dimensional parameter computed based on the values of k and P
$C_{\varepsilon 3}$	0.2
d	grain size
D_k	diffusion term
f_i	Reynolds stresses for which a turbulence model is required for closure
F	fluid fraction function
g	acceleration due to gravity
G	buoyancy production term
h	tailwater depth
h_m	predicted maximum depth of the scour hole
h_m'	observed maximum depth of the scour hole
H	difference in height from water level upstream of the weir to the tailwater level
k	turbulent kinetic energy
K	scour coefficient for rock bed
l	apron length
L	length of a rock block
N_j	number of joint sets
P	turbulence production term
P'	pressure
q	unit discharge over structure

doi: 10.2166/hydro.2014.105

R hydraulic radius of jet
r CC
RQD rock quality designation
s end sill height
t time
u velocity in x direction
v velocity in y direction
w velocity in z direction
w_s mean particle fall velocity
V_j jet velocity impinging on the tailwater
V_F volume fraction of fluid in each cell
V average velocity which is equivalent to the square root of the square of u plus the square of v
V_m maximum average flow velocity
z fall height
α dip angle of joint set j
β air content
γ_j residual friction angle of joint set
θ jet angle
ε energy dissipation rate
μ dynamic viscosity
ν kinematic viscosity of water
ρ_s mass density of sediments
ρ mass density of the averaged volume fraction
σ sediment nonuniformity
σ_c uniaxial compressive strength
σ_k 0.72 in the RNG k-ε model
σ_t uniaxial tensile strength
σ_ε 0.72 in the RNG k-ε model

ABBREVIATIONS

CC correlation coefficient
CFD computational fluid dynamics
FAVOR fractional area/volume obstacle representation
GA genetic algorithm
LM Levenberg–Marquardt
PSO particle swarm optimisation
RANS Reynolds-averaged Navier–Stokes
RMSE root mean square error
RNG renormalisation-group
RQD rock quality designate
SA simulated annealing
VOF volume of fluid

INTRODUCTION

High-speed water jets originating from spillways often cause considerable scour downstream of a hydraulic structure. The scouring process continues until the shear stress exerted by the impinged water is incapable of dislodging and removing bed material due to the increased water depth in the scour hole (Guven & Azamathulla 2012), which corresponds to the maximum scour depth, h_m. Scouring can endanger the safety of the dam and the adjoining structures. Therefore, a prediction of the maximum scour depth (h_m) is of high significance in any spillway design.

Numerous investigators have concentrated their efforts on developing empirical formulae, which are very convenient to use during preliminary design stages (Bollaert & Schleiss 2003). Some major formulae used for scour depth prediction are shown in Table 1 (all symbols in Table 1 are defined in the 'Notation' section above). Table 1 illustrates that various hydraulic, morphologic and geotechnical factors affect the maximum scour depth (Guven & Azamathulla 2012) but only three of these variables, namely, the discharge per unit (q), water head (H) and particle size (d) are commonly reported in most references. However, other factors are necessary to obtain accurate predictions (Azamathulla *et al.* 2005), and the trend in recent studies to consider more factors is observed in Table 1. Independent of the factors considered, empirical equations simplify the complex scouring process, and prototype conditions are commonly approximated and averaged; therefore, the maximum scour depth prediction may be far from the actual values (Guven & Azamathulla 2012). Recently, soft computing techniques, including genetic programming (Azamathulla *et al.* 2008b), gene-expression programming (Guven & Azamathulla 2012), and artificial neural networks (Azamathulla 2006; Azamathulla *et al.* 2005, 2008a) have proven more efficient in predicting scour than conventional formulae. Extensive data on spillway bucket erosion in the recent papers noted above are widely available for predicting the scour depth downstream from ski-jump spillways (Azamathulla 2013).

Table 1 | Existing formulae to evaluate ultimate scour depth and a summary of the morphologic, hydraulic and geotechnical parameters

						Geotechnical factors	
Type	**Year**	**Author(s)**	**Time**	**Morphologic factors**	**Hydraulic factors**	**Gran. soil**	**Jointed rock mass**
Empirical	1932	Schoklitsch			q, H	d	
	1937	Veronese A			q, H	d	
	1937	Veronese B			q, H		
	1939	Jaeger			q, H, h	d	
	1953	Doddiah *et al.*	t		q, H	d, w_s	
	1957	Hartung			q, H, g	d	
	1963	Rubinstein			H, h, g, V_j, θ, C		L
	1966	Damle *et al.*			q, H		
	1967	Kotoulas			q, H	d	
	1969	Chee & Padiyar			q, H	d	
	1974	Chee & Kung			q, H, g, θ	d	
	1973	Martins A			q, H, h, θ		L
	1975	Martins B			q, H		
	1978	Taraimovich			H, V_j, θ	w_s	
	1982	Incyth			q, H		
	1982	Machado A			q, H, g, C	d	
	1982	Machado B			q, H, g, C		
	1985	Mason & Arumugam			q, H, h, g	d	
	1989	Mason			q, H, h, g, β	d	
	2003	Canepa & Hager (2003)			V_j, g, β	d	
	2006	Azamathulla *et al.* (2006)			q, H		
	2006	Dey & Sarkar (2006)		b_g, l	h, g, V_j, ν	d, ρ_s	
	2006	Pagliara *et al.*			h, g, V_j, θ, β	d, ρ_s, σ	
	2011	Oliveto *et al.* (2011)	t	l, s	q, g, h, ν	d, ρ_s, σ	
	2012	Ghodsian *et al.* (2012)		b_w, B	H, h, g, V_j, R	d, ρ_s	
Semi-empirical	1960	Mikhalev			q, H, h, g, θ, β	d	
	1963	Chen (1963)			q, H		K
	1963	Yu			q, H		K
	1967	Mirtskhulava *et al.*			q, H, h, g, V_j, θ, C	w_s, ρ_s	σ_c, σ_t, L
	1967	Poreh & Hefez			q, H, V_j	d, ρ_s	
	1975	Zvorykin			h, V_j, θ		
	1983	Mih & Kabir			h, g, V_j, θ	d, ρ_s	
	1985	Chee & Yuen			h, g, V_j, θ	d, ρ_s	
	1985	Spurr	t		q, H, h, g, V_j, θ	d	σ_c, σ_t, RQD, N_j, L, α
	1991	Bormann & Julien			q, g, V_j, θ	d, ρ_s	
	1994	Fahlbusch			q, h, g, V_j, θ, β	d	σ_c, σ_t
	1998	Annandale *et al.*			q, H, h, g, V_j, θ, β	d, ρ_s	σ_c, σ_t, RQD, N_j, L, α, γ_j

(*continued*)

Table 1 | continued

Type	Year	Author(s)	Time	Morphologic factors	Hydraulic factors	Geotechnical factors: Gran. soil	Geotechnical factors: Jointed rock mass
	1998	Hoffmans			$q, h, g, V_j, \theta, \beta$	d, ρ_s	
	2003	D'Agostino & Ferro		b_w, B, z	H, h	d	
	2005	Liu (2005)			q, H, h, θ, b_j		K
	2007	Liu & Li			q, H	d	K
Standards	1985	Bureau of Indian Standards (1985)			q, H		
	2005	Standard of Ministry of Water Resources, PRC			q, H		K

Note: All symbols are defined in the 'Notation' section.
References from before 2003 are given in Bollaert & Schleiss (2003); the other references are listed at the end of the paper.

Other researchers have tried to develop physical models and numerical methods. Physical models were considered to be more sensitive to scale effects (Spurr 1985). Thus, some researchers have studied numerical models for the erosion of loose beds (Liu & Garciá 2006; Huai *et al.* 2011). However, the physical mechanism of rock disintegration and scour pool formation is more complex in rock beds than in loose beds (Li & Liu 2010). No commercial computational fluid dynamics (CFD) software is currently available to simulate the scouring process of a rocky bed. Fortunately, any CFD code can simulate the complicated phenomenon caused by multiple crossing jets, irregular jet shapes and complex geometries, such as stepped spillways, whereas the conventional formulae are not appropriate for these situations. Moreover, discovering that scour is related to the turbulent flow structures calculated by any CFD software is exciting (Haltigin *et al.* 2007). Bey *et al.* (2007) found that sweep and ejection type events can potentially contribute to scour. Termini & Sammartano (2012) carried out some experiments to understand the role of flow turbulence in predicting the scouring process and sediment movement on the basis of detailed measurements of flow velocity in the scour hole region. Ge *et al.* (2005) found that regions of maximum shear velocity correspond to the maximum scour depths in the shear zone, and that numerical values of vertical velocity are very important in explaining scour and deposition patterns. However, the relationship between maximum velocity and maximum scour depth is still unknown.

The aim of this study is to provide a new formula for estimating the maximum depth of scour on a rocky bed due to the high-speed water jets from overflow dams. The formula is based on the CFD technique, the use of which is the biggest difference between the present technique and traditional equations. More accurate predictions can be obtained from this new formula because the CFD technique considers the complex hydraulic and morphological conditions that conventional formulae are not able to consider, even when using more factors. First, the numerical methodology for analysing the three-dimensional flow field of the overflow dams is introduced and validated using experiments. Subsequently, the relationship between the maximum numerically simulated velocity based on CFD and the maximum scour depth is studied using the Levenberg–Marquardt (LM) algorithm, and a new prediction formula is established. The accuracy of this formula is compared with the accuracy of three other conventional equations. Finally, the proposed formula is applied to the Wuqiangxi project. This achievement is useful for obtaining accurate predictions for the design of overflow dams and plunge pools.

NUMERICAL METHODOLOGY

Flow-3D developed by Flow Science, Inc., Santa Fe, New Mexico, uses the finite-volume method to solve the

Reynolds-averaged Navier–Stokes (RANS) equations and is applied to complete the numerical simulation. The Cartesian computational domain is subdivided into a grid of hexahedral cells. Within each cell are the associated average values of all of the dependent variables at the centre of each cell, except for velocities u, v and w and the fractional areas A_x, A_y and A_z, which are located at the cell-faces. The staggered grid technique is used to compute the average values of the flow parameters (pressure and velocity) at discrete times. The renormalisation-group (RNG) k-ε turbulent transport model, which simulates the anisotropy of high-speed jets very well, is used for turbulence closure. A computer-generated object of the whole solid region containing the weir, the energy dissipater, the stilling basin and the banks is imported into Flow-3D. The object is defined as an obstacle in the rectangular domain by the implementation of the fractional area/volume obstacle representation (FAVOR) method. The volume of fluid (VOF) method is employed for computing the free surface.

Geometry representation

To define any complex geometry for the finite control volume, the FAVOR method, as outlined by Hirt & Sicilian (1985), is used. The FAVOR method is a porosity technique that catalogues cells between 0 and 1 and expresses the fraction occupied by an object (resulting in 0 within obstacles and 1 for cells without an obstacle). Therefore, the solid surface is defined by the cells within the grid that have a porosity value between 0 and 1. A first-order approximation, a straight line in two dimensions and a plane in three dimensions, is determined by the points where the obstacle intersects the cell faces and is used to define the location of the interface. This slicing plane defines the fractional area (A_x, A_y and A_z) on each cell face that fluid can flow through, as well as the fractional volume that can contain fluid. The 'stair-stepping' effect normally related to rectangular grids is eliminated through this method. All of the obstacle surfaces, curved or otherwise, are replaced with short, straight-lined segments. Given this fact, the FAVOR method is limited by the resolution of the computational grid, and smaller sized cells produce a much smoother numerical obstacle boundary.

Free surface

To numerically solve the rapidly varying flow over the spillway and dissipater, tracking the free surface accurately is important. The VOF method is an effective way to handle a complex free water surface (Zhang *et al.* 2011). This method consists of three main components: defining the function for the VOF, solving the VOF transport equation and setting the boundary conditions at the free surface. The fluid fraction function F is defined to be equal to 1 in the fluid, 0 in the void, and a value between 0 and 1 in partially filled cells. The fluid interface is reconstructed in 3D using a piecewise linear representation, where the interface is assumed to be planar in each cell containing the interface. The fluid volume bounded by the interface and cell faces is then moved according to the local velocity vector in a Lagrangian manner. Finally, the advected volume is overlaid back onto the Eulerian grid to obtain the new values of the fraction-of-fluid function. Once again, the first-order approximation is not an exact fit to the curved flow surface, but many researchers have demonstrated that Flow-3D is capable of reasonably predicting the flow field of a spillway, provided that the disposal approach is reasonable, including the mesh resolutions, turbulence options, boundary conditions and numerical options (Johnson & Savage 2006).

Governing equations

The general governing continuity and RANS equations for incompressible flow, including the FAVOR and VOF variables, are as follows.

Continuity equation

$$\frac{\partial}{\partial x}(uA_x) + \frac{\partial}{\partial y}(vA_y) + \frac{\partial}{\partial z}(wA_z) = 0 \tag{1}$$

Momentum equation

$$\frac{\partial U_i}{\partial t} + \frac{1}{V_F}\left(U_j A_j \frac{\partial U_i}{dx_j}\right) = \frac{1}{\rho}\frac{\partial P'}{dx_i} + g_i + f_i \tag{2}$$

where t is the time, and u, v and w represent the velocities in the x-, y- and z-directions; V_F is the volume fraction of fluid in each cell; A_x, A_y and A_z are the fractional areas open to

flow in the subscript directions; ρ is the density; P' is the pressure; g_i is the gravitational force in the subscript direction; and f_i represents the Reynolds stresses for which a turbulence model is required for closure.

Turbulence model

The RNG method applies statistical methods for a derivation of the averaged equations for the turbulent kinetic energy (k) and the turbulent kinetic energy dissipation rate (ε). The RNG-based models rely less on empirical constants while setting a framework to derive a range of parameters to be used at different turbulence scales. The empirically determined equation constants in the standard k-ε model are derived explicitly in the RNG model. The RNG k-ε turbulent transport equations are as follows.

k-equation

$$\frac{\partial k}{\partial t}+u\frac{\partial k}{\partial x}+v\frac{\partial k}{\partial y}+w\frac{\partial k}{\partial z}=P+G+D_k-\varepsilon \tag{3}$$

where k is the turbulent kinetic energy, ε is the energy dissipation rate, and P is the turbulence production term. This turbulence production term is represented in Cartesian coordinates as

$$P=\frac{C_{\mathrm{sp}}\mu}{\rho}\left[2\left(\frac{\partial u}{\partial x}\right)^2+2\left(\frac{\partial v}{\partial y}\right)^2+2\left(\frac{\partial w}{\partial z}\right)^2+\left(\frac{\partial v}{\partial x}+\frac{\partial u}{\partial y}\right)^2+\left(\frac{\partial u}{\partial z}+\frac{\partial w}{\partial x}\right)^2+\left(\frac{\partial v}{\partial z}+\frac{\partial w}{\partial y}\right)^2\right] \tag{4}$$

where μ is the dynamic viscosity, and C_{sp} is the shear production coefficient. In Equation (3), G is the buoyancy production term

$$G=\frac{\mu}{\rho^3}\left[\frac{\partial \rho}{\partial x}\frac{\partial p}{\partial x}+\frac{\partial \rho}{\partial y}\frac{\partial p}{\partial y}+\frac{\partial \rho}{\partial z}\frac{\partial p}{\partial z}\right] \tag{5}$$

The diffusion term in Equation (3), D_k, is

$$D_k=\frac{\partial}{\partial x}\left(\frac{\nu}{\sigma_k}\frac{\partial k}{\partial x}\right)+\frac{\partial}{\partial y}\left(\frac{\nu}{\sigma_k}\frac{\partial k}{\partial y}\right)+\frac{\partial}{\partial z}\left(\frac{\nu}{\sigma_k}\frac{\partial k}{\partial z}\right) \tag{6}$$

where ν is the turbulent viscosity, and $\sigma_k=0.72$ in the RNG k-ε model.

ε-equation

$$\frac{\partial \varepsilon}{\partial t}+u\frac{\partial \varepsilon}{\partial x}+v\frac{\partial \varepsilon}{\partial y}+w\frac{\partial \varepsilon}{\partial z}=C_{\varepsilon 1}\frac{\varepsilon}{k}(P+C_{\varepsilon 3}G)+D_\varepsilon-C_{\varepsilon 2}\frac{\varepsilon^2}{k} \tag{7}$$

where $C_{\varepsilon 1}$, $C_{\varepsilon 2}$ and $C_{\varepsilon 3}$ are user-adjustable, non-dimensional parameters. The default value for $C_{\varepsilon 1}$ is 1.42. $C_{\varepsilon 2}$ is computed based on the values of k, and P. $C_{\varepsilon 3}$ is 0.2. The diffusion term for the dissipation is

$$D_\varepsilon=\frac{\partial}{\partial x}\left(\frac{\nu}{\sigma_\varepsilon}\frac{\partial \varepsilon}{\partial x}\right)+\frac{\partial}{\partial y}\left(\frac{\nu}{\sigma_\varepsilon}\frac{\partial \varepsilon}{\partial y}\right)+\frac{\partial}{\partial z}\left(\frac{\nu}{\sigma_\varepsilon}\frac{\partial \varepsilon}{\partial z}\right) \tag{8}$$

where $\sigma_\varepsilon=0.72$ in the RNG k-ε model.

For an unbalanced current, especially when secondary currents are flowing, the RNG model with revised coefficients provides lower diffusion than the standard model. In other words, this model expresses that the predicted viscosity values will usually be increased.

VALIDATION OF THE NUMERICAL MODEL

Numerical model implementation

The simulated object in the mathematical model is combined with a practical project. The flood discharging section includes three crest overflowing orifices in the middle and two mid-discharge orifices on either side. As shown in Figures 1 and 2, the drop elevations of the crest overflowing orifices and mid-discharge orifices are 1,598.0 and 1,540.0 m, respectively. Additionally, the drop heights are 165.0 and 107.0 m for the crest overflowing orifices and mid-discharge orifices, respectively. The check water level is 1,622.73 m, and the discharge is 13,854 m^3/s. The stilling basin is 170.0 m long and 78.0 m wide. The elevation of the stilling basin slab is 1,433.0 m. The tailwater level is 1,496.513 m. The location for the upstream boundary is 50 m upstream from the crest, and the downstream boundary is placed downstream of the stilling basin, where the boundary has no effect on the computation. The numerical simulation covers the flood discharging section, the headwater reservoir, the stilling basin and the downstream

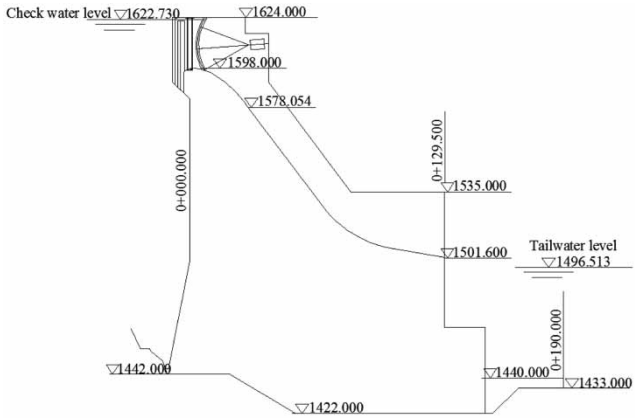

Figure 1 | Longitudinal section of the crest overflowing orifice.

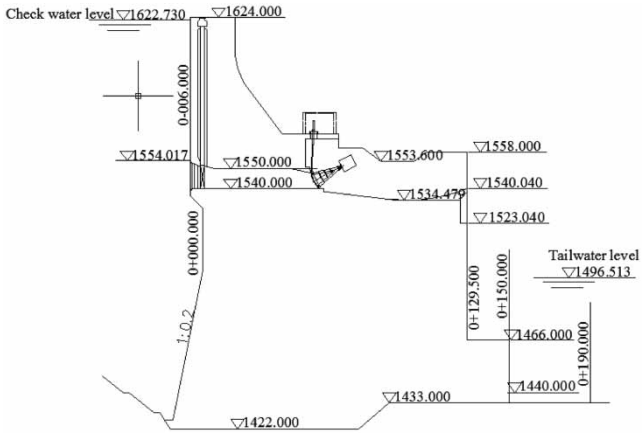

Figure 2 | Longitudinal section of the mid-discharge orifice.

reach. The whole model is spatially discretised in a multi-block pattern. Each block spans a certain region of the whole flow domain and contains the standard structured rectangular mesh. The calculation region and the multi-block meshes of the model are shown in Figures 3 and 4, respectively.

The boundary conditions are as follows.

- Upstream boundary: hydrostatic pressure with zero velocity; a fluid height of 200.73 m is used for the stagnation pressure boundary condition.
- Downstream boundary: hydrostatic pressure with zero velocity; fluid height of 61.513 m is used for the stagnation pressure boundary condition.
- Top boundary: symmetry.

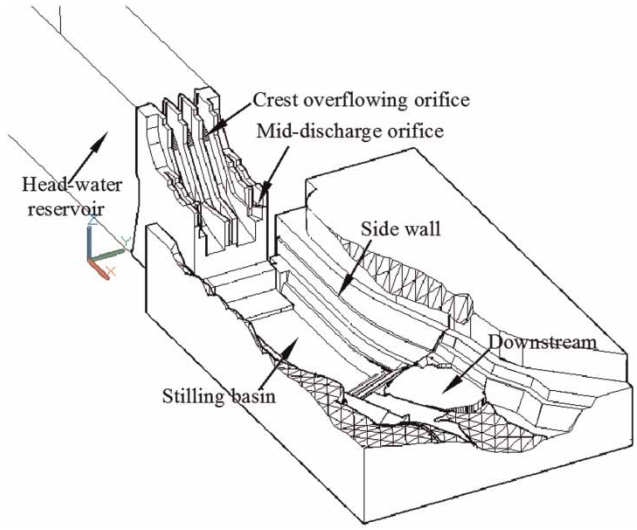

Figure 3 | Numerical simulation region.

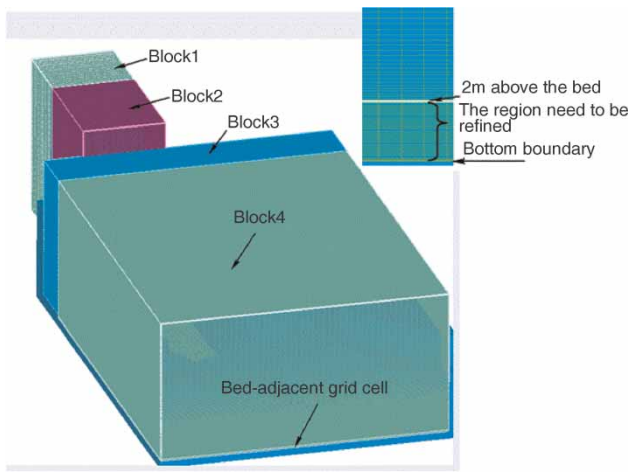

Figure 4 | Mesh of the simulated region.

- Bottom boundary: no slip/wall; no slip is defined as zero tangential and normal velocities ($u = v = w = 0$).
- Sidewalls: symmetry.

An accurate representation of the flow near the bottom of the stilling basin leads to a successful prediction of the scour. To research the sensitivity of the computed solutions to grid refinement, computations on three grids are carried out. The difference in the three schemes is the fineness of the bed-adjacent grid cells in the region 2 m above the bed surface, as shown in Figure 4. A cell size of approximately $\Delta x = \Delta y = \Delta z = 1$ m is adopted in other regions. The cell sizes in the region 2 m above the bed are 0.2, 0.1 and

0.05 m for the total active cell counts of 5.2, 6.4 and 8.8 million, respectively. The steady-state x direction velocity component u, y direction velocity component v, and horizontal velocity V ($V = (u^2 + v^2)^{1/2}$) of 38 points uniformly distributed along the midline of the mid-discharge orifice near the bed are calculated as shown in Figure 5. Vertical velocities for the three meshes should not be compared because the z-velocities of the 38 points are all smaller than 0.5 m/s. The results of the three meshes have exceptionally consistent values, and the errors of the 0.1-m mesh and 0.2-m mesh are smaller than 10% compared with the results of the model using the 0.05-m mesh. The refined mesh (0.05 m) was not used because this mesh requires too many cells and because it has been proven to provide results almost coincident with the results of the 0.1-m mesh. In this case, considering the accuracy and the computation time, the model with the 0.1-m mesh (the total active cell counts are 6.4 million) can be used to calculate the flow phenomenon and the velocities near the bed.

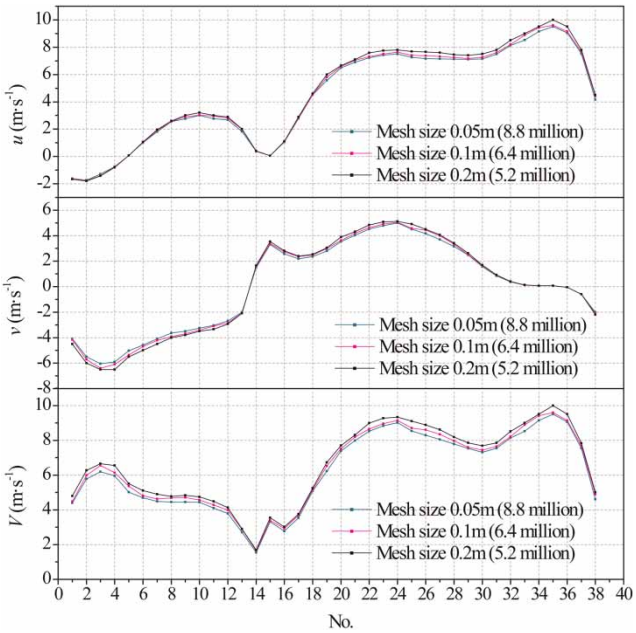

Figure 5 | Velocities of the 38 points uniformly distributed along the midline of the mid-discharge orifice near the bed.

VERIFICATION RESULTS

The aim of this study was to use the output of the simulated flow field over a flat rock bed to predict the maximum depth of the scour hole. A physical model of the project at a 1/100 scale was constructed at Kunming hydropower investigation, Design and Research Institute, HECC, for the purpose of verifying the 3D numerical model. The geometry of the physical model was the same as the numerical model, which is clearly described in the section 'Numerical model implementation'. The tests and numerical simulations had long durations to achieve quasi-equilibrium conditions. Figure 6 shows the flow regimes obtained from the model

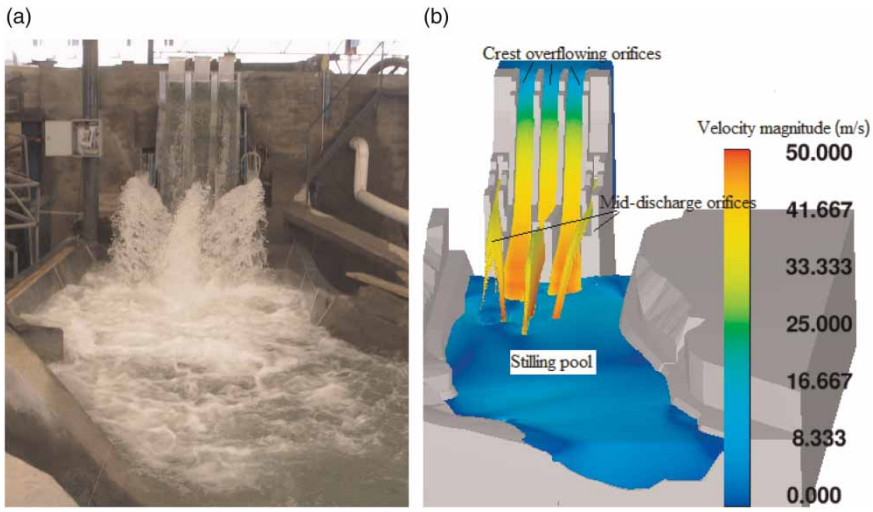

Figure 6 | Water flow regime: (a) hydraulic model test; (b) numerical simulation.

test (a) and the numerical simulation (b), and the regimes match reasonably well. The flow from the middle crest overflow orifice with a slot dissipator narrowed immediately and expanded vertically. The flow from the two side crest overflow orifices with micro-diffusion energy dissipators had slight lateral diffusion, while the two mid-discharge orifices slanted the flow towards the centre of the river bed. Figure 7 shows the distributions of the 221 measured points at a horizontal plane very close (0.1 m) to the channel bottom. The vertical velocities of the 221 points are all smaller than 0.5 m/s, indicating that the horizontal flow along the flat bed appears slow. The steady-state fluid average velocity V is defined as the square root of the square of u plus the square of v, i.e. $V = (u^2 + v^2)^{1/2}$. The comparison of the measured and simulated velocities of all 221 points, as shown in Figure 8, indicates that the results from CFD are in good agreement with the physical model, and the root mean square error (RMSE) is 1.0246. The greatest absolute deviation between the numerical simulation and the scaled physical model data for these points is 0.5 m, and this result occurs at point 20 on line 5. The relative error of this deviation is 6.6%. The CFD method effectively simulates the flow field and the velocity distraction of overflow dams.

The effect of the jet air content on the plunge pool scour remains a challenge because of the limitations in current research methodology and the random and chaotic character of air entrainment, and is not considered in this study nor in most of the existing methods (D'Agostino & Ferro 2003; Liu & Li 2007).

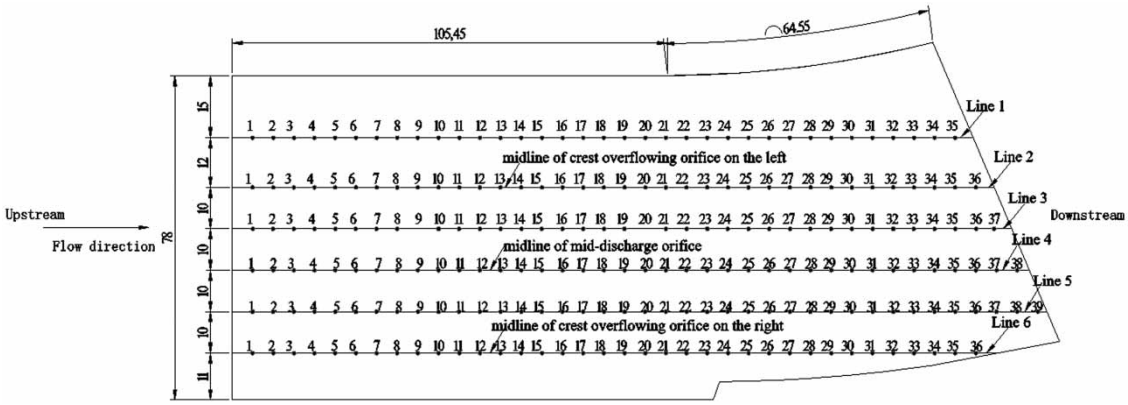

Figure 7 | Planform of the plunge pool showing the location of the points (the total number is 221).

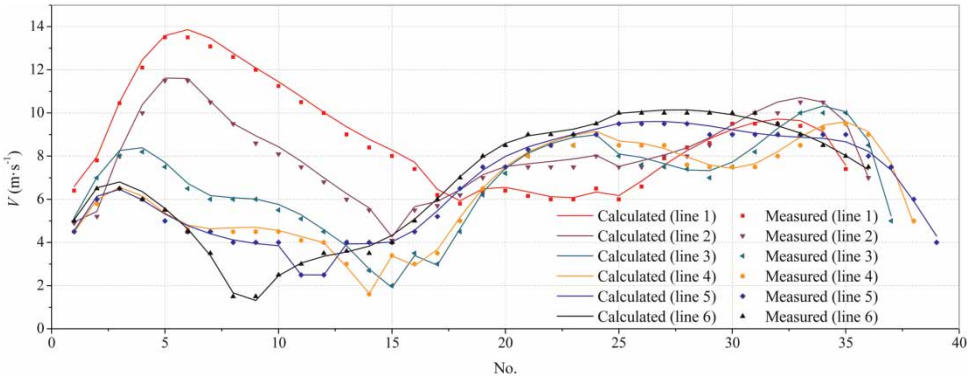

Figure 8 | Measured and calculated velocities of the 221 points near the bed.

PREDICTION FORMULA FOR ROCKY BED SCOUR BASED ON CFD

Proposed formula based on CFD numerical methodology

The submerged impinging jet flow is divided into a free jet region, a jet impingement region and a wall jet region (Beltaos & Rajaratnam 1973). Deng *et al.* (2002) concluded that bed rocks were mainly broken under the effect of pulsed pressure in the impingement region (Bollaert & Schleiss 2005; Li & Liu 2010), but the process of scouring occurred due to the effect of velocity in the wall jet region. The pockets of large shear velocity correlate well with the region of maximum scour depth (Ge *et al.* 2005), and the scour hole is deepest where strong downwelling is prevalent (Haltigin *et al.* 2007). For continuity to be satisfied, the strong downwelling must be accompanied by a large horizontal flow along the bed directed away from the dam, tending to sweep bed material away from the riverbed and promote scour. Scour occurs at velocities up to the threshold velocity. As a result, the maximum scour depth is related to the maximum horizontal flow velocity near the bed, but the exact relationship is difficult to understand.

The empirical formulae regarding the scour depth prediction in most literature have the same form (Liu & Li 2007)

$$h_m = K\frac{q^x H^y}{d^z} \tag{9}$$

where x, y and z are the indexes; h_m is the maximum scour depth; K is the scour coefficient of rock; q is the unit discharge over structures; H is the difference in height from the water level upstream of the weir to the tailwater level; d is the diameter of the bed material.

The two parameters q and H in Equation (9) represent the magnitude of the erosive power of the plunging jet and should be replaced by parameter V_m, showing that the erosive power of the plunging jet on the stilling basin is obtained from CFD models. K and d indicate the scour resistance offered by the rock. Many methods (Pagliara *et al.* 2006) consider the rock bed as a completely disintegrated rock bed simulated with non-cohesive granulates of grain size d; therefore, this assumption cannot be transferred to the prototype scour of the rocky riverbed (Manso *et al.* 2004). Actually, the riverbed does not completely disintegrate due to the geometric characteristics and cohesive forces of the rocks. The scour coefficient of the bedrock, K, is a composite and simple parameter and is related to the geometry, the mechanical properties, the fissure formation, and the cemented situation of the bedrock. As the value of K increases, the erosion resistance of the bedrock decreases. Nevertheless, determining this coefficient theoretically is very difficult. According to the Standard of Ministry of Water Resources PRC (2005), bedrock can be divided into four classes according to the situation of the jointed rock cracks and the structural characteristics of the bedrock. The corresponding ranges of K for different classes of bedrock are shown in Table 2. Based on Table 2 and field observations, the recommended values for K are given for each project. In this paper, K is chosen to represent the scour resistance offered by the rock.

Table 2 | Range of the scour coefficient of bedrock K

Class	Structure character of bedrock in scour pit	K values	
		Range	Average
I (Hard to scour)	Huge block; joints undeveloped and obturated; anti-erosion velocity >12 m/s	0.6–0.9	0.80
II (Difficult to scour)	Big block; joints developed, most obturated, with a little filling; 12 m/s ≤ anti-erosion velocity <8 m/s	0.9–1.2	1.10
III (Easy to scour)	Block fractured; joints developed and most splaying, with a little filling; 8 m/s ≤ anti-erosion velocity <5 m/s	1.2–1.6	1.4
IV (Rather easy to scour)	Block pieces; joints fully developed; cranny splaying entirely or partly; with some clay filling; anti-erosion velocity ≥5 m/s	1.6–2.0	1.8

Establishing a regression model includes collecting predictor (independent variables) and response (dependent variables) values for the samples and then fitting a predefined mathematical relationship to the collected data. A power-law form, such as Equation (9), is adopted to express the relationship between the simulated flow velocity over a flatbed (V_m), the non-dimensional scour coefficient (K), and the resulting equilibrium scour depth (h_m). The acceleration due to gravity, g, is also incorporated and makes possible a dimensional balance, giving the form of the expression as shown in Equation (10)

$$h_m = a\left(\frac{V_m^2}{g}\right)^b K^c \tag{10}$$

where a, b and c are the exponents, h_m is the dependent variable, and V_m and K are the independent variables.

Data collection

Because most of the empirical or semi-empirical approaches for modelling rock scour have been developed based on scaled model experiments and exhibit significant scaling effects when applied to prototype cases (Bollaert & Schleiss 2005), the available measurement data in the actual cases were surveyed. This survey showed that five types of information in 24 projects (Liu 1994) in China, namely, scour depth below the initial bed (h_m'), fall height (H), discharge intensity (q), tail water depth (h), and the scour coefficient of rock bed (K), have been reported. Based on the numerical methodology studied earlier, numerical models of the 24 projects were built according to the engineering data to obtain the maximum velocity, V_m, near the bed surface. The CFD models were all run until a steady flow was achieved. Table 3 shows the data used for solving the unknown exponents a, b and c in Equation (10). The first 18 datasets (75%) were chosen for model training, and the remaining six datasets (25%) were used for testing.

Regression analysis

The appropriate values of a, b and c in Equation (10) were obtained using four types of modern optimisation algorithms on the training sets: LM, genetic algorithm (GA), simulated annealing (SA) and particle swarm optimisation (PSO). The optimisation software package, 1stOpt, was applied to execute these algorithms. 1stOpt was developed by 7D Software High Technology Inc., and this software is a robust, easy-to-use and powerful optimisation tool that can be used widely in various engineering fields (Guan *et al.* 2010). To select the most suitable option of these algorithms, the correlation coefficient (CC) and RMSE were compared for the results with the different algorithms, as shown in Table 4. The results show that the four algorithms align reasonably well. LM provides the smallest value for the RMSE and the highest value for the CC, making this technique the obvious selection for the final results.

Table 3 | Data used

	Measured data					
					Rock scour coefficient	Simulated data
No.	Fall height H/m	Discharge intensity q/(m^2 s^{-1})	Tail water depth h/m	Depth of scour h_m'/m	K	Velocity V_m/(m s^{-1})
1	34.60	47.00	10	19.00	1.74	16.90
2	35.94	49.00	14.1	17.30	1.83	14.10
3	21.92	17.70	5.55	8.40	1.53	11.50
4	69.00	23.50	7.1	1.00	0.58	19.60
5	70.30	40.10	4	13.10	0.93	28.70
6	58.32	23.60	3.8	3.30	0.53	24.20
7	58.32	22.20	4.8	4.90	0.74	21.70
8	58.32	22.20	5.3	8.20	0.85	21.10
9	55.86	33.70	2.9	13.10	1.01	26.80
10	45.00	56.00	15.34	4.86	1.04	16.80
11	56.50	60.00	5.1	25.10	1.42	28.80
12	18.60	11.30	3	3.00	0.86	14.00
13	30.60	46.00	12.4	5.00	1.09	14.50
14	20.30	50.00	4.8	20.60	1.69	19.70
15	33.77	49.30	14.14	18.04	1.91	13.80
16	66.57	84.80	9.43	18.98	1.09	29.80
17	56.50	60.00	5.00	25.10	1.42	29.70
18	38.40	43.80	2.94	16.00	1.15	24.80
19	30.60	46.00	11.86	5.54	1.09	14.70
20	90.00	79.66	18.00	31.00	1.78	21.60
21	57.25	48.30	6.14	12.80	0.99	25.50
22	69.03	42.50	7.15	13.00	1.07	23.00
23	45.68	46.10	13.34	6.60	1.13	15.00
24	30.45	61.80	11.90	8.53	1.11	17.90

Table 4 | Accuracy measures evaluated for LM, GA, SA and PSO on the training set

Algorithms	a	b	c	CC	RMSE
LM	0.78067373	0.64538814	1.80013043	0.9851702966	1.34465307388003
GA	0.78067366	0.64538815	1.80013049	0.9851702957	1.34465307388004
SA	0.78064422	0.64539641	1.80014566	0.9851700041	1.34465307549369
PSO	0.77926292	0.64570247	1.80177915	0.9851477083	1.34466177352218

The non-linear curve fitting equation using LM is

$$h_m = 0.781\left(\frac{V_m^2}{g}\right)^{0.645} K^{1.8} \quad (11)$$

$g = 9.80665\ \mathrm{m/s^2}$ and is then substituted into Equation (11), and the simple form is obtained as Equation (12)

$$h_m = 0.179 V_m^{1.29} K^{1.8} \quad (12)$$

The RMSE of this formula is 2.02, and the CC, r, is 0.9852, implying that this formula has a satisfactory goodness of fit and that the two variables explain the maximum scour depth. This result is expected because the flow field characteristics as well as the rock properties have significant influences on the bed erosion.

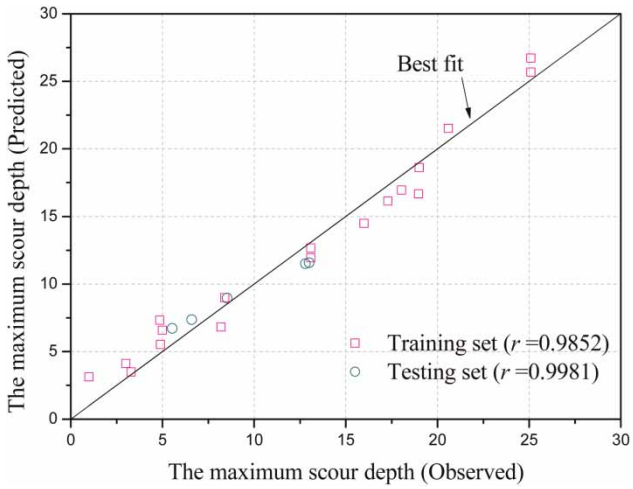

Figure 9 | Predicted and observed maximum scour depth for training and testing sets.

Validation of the proposed formula

The validation of Equation (12) is verified using the remaining six sets of data. Validation of the trained model proves that the proposed formula is highly generalisable, having a high correlation (CC $r = 0.9981$) and low RMSE (1.775). As shown in Figure 9, almost all of the estimations from the formula fall on the line in perfect agreement with the data, showing good agreement with the observed data.

Chen's formula, Martins' formula and the Veronese formula are suggested in the Bureau of Indian Standards, and are as follows:

$$h_m = 1.25 q^{0.5} H^{0.25} - h \quad (13)$$

$$h_m = 1.5 q^{0.6} H^{0.1} - h \quad (14)$$

$$h_m = 1.9 q^{0.54} H^{0.225} - h \quad (15)$$

As a further check, the performance of Equation (12) and also Equations (13)–(15) are compared based on the training and testing sets, as shown in Figure 10. The overall best performance of the proposed model is shown in Figure 10, with the lowest values of the error measure (RMSE = 2.5458) and the highest correlation ($r = 0.9828$). Almost all estimations by the Veronese formula are observed to be larger than the measured values. The results from Martins' formula and Chen's formula tend to provide consistent predictions. However, the Veronese formula estimates scour depth much better than Martins' formula and Chen's formula based on the r value, but Martins' formula provides a better estimate than the other two in terms of a lower RMSE. Relative errors of the proposed formula with the other three formulae are shown in Figure 11. The observed maximum scour depth of the fourth project is only 1.00 m, and the relative errors of the predictions by

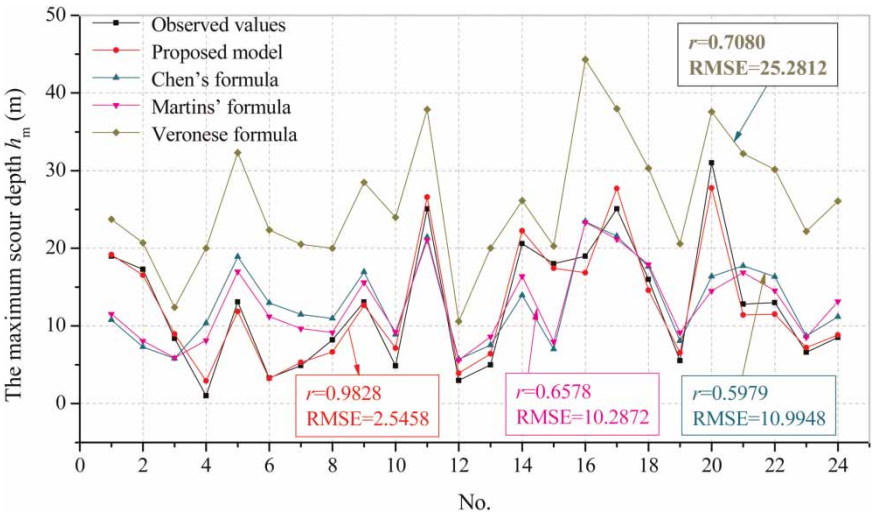

Figure 10 | Observed and predicted maximum scour depth for training and testing sets.

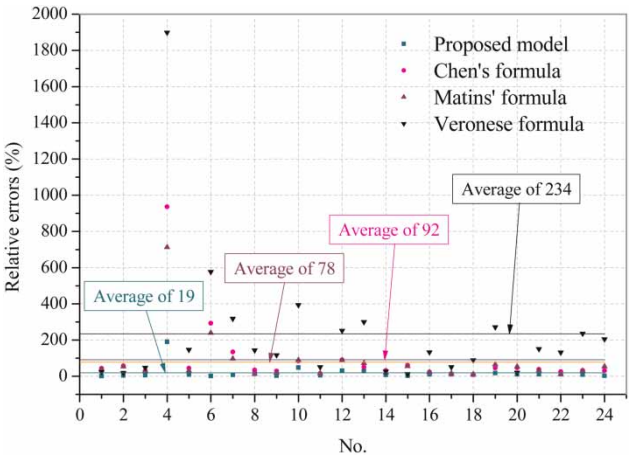

Figure 11 | Relative errors of the proposed formula, with the other three formulae.

the formulae are the largest errors in this project. The average relative error of the proposed formula is 19%, whereas the error for Chen's formula is 92%, that of Martins' formula is 78% and the Veronese formula is 234%. In general, the proposed formula in this study based on CFD can effectively predict the maximum scour depth of a rocky bed downstream of overflow dams.

APPLICATION IN THE WUQIANGXI PROJECT

Wuqiangxi Hydropower Station, which is located in Yuanling County in the western part of Hunan province, China, encountered the heaviest flood on record in July 1996. The maximum flow rate in the reservoir was 43,100 m^3/s (nearly a 100-year flood), the controlled discharge flow rate was 26,400 m^3/s, the water level upstream reached 113.26 m (equivalent to the 5000-year flood elevation), and the tailwater level was 67.40 m (equivalent to the 20-year flood elevation). The flood discharging section on the right side of the dam includes three crest overflowing orifices. The longitudinal section diagram is shown in Figure 12, and the width of the stilling pool is 72.00 m. The No. 1 and No. 3 orifices were at local opening conditions, specifically, the opening of the arc gate was 5.0 m, the discharge of each hole was 1,840 m^3/s, and the unit discharge was 97 m^2/s. However, the middle gate, the No. 2 orifice, was fully open, and the highest water head above the weir crest was 25.45 m, the discharge was 5,300 m^3/s, and the unit discharge was 279 m^2/s. The right stilling pool base slab suffered severe damage, and along the midline of the No. 2 orifice a scour pit appeared 50 m in length, 16 m in width, and 13–36 m in depth. The shape of the scour pit and the repair measures are shown in Figure 13 (Lian & Yang 2008).

Based on the data from the Wuqiangxi project, the anti-erosion velocity of the rock in the cushion pool reaches approximately 5 to 6 m/s (Lian & Yang 2008). According to Table 2, the rock class is between III (Easy to scour) and IV (Rather easy to scour), and the scour coefficient, K,

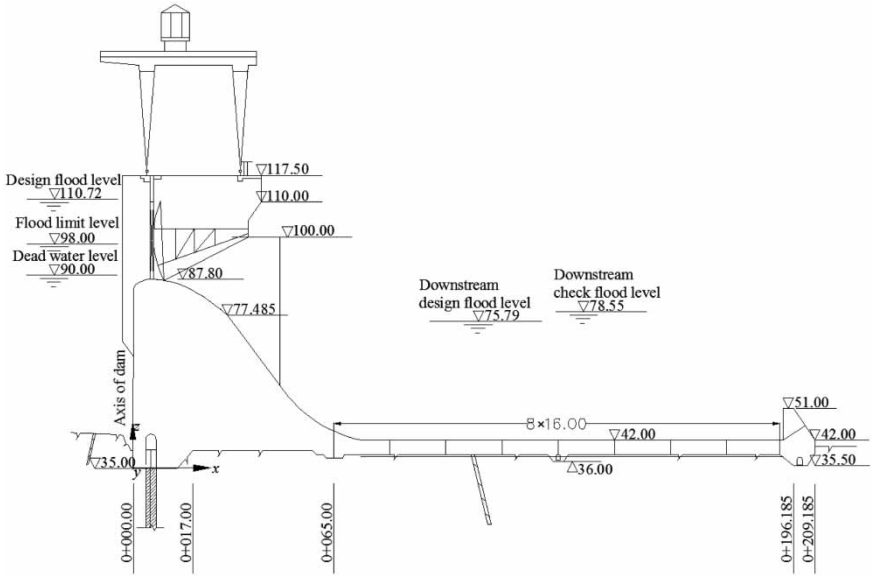

Figure 12 | Longitudinal section of the crest overflowing orifice.

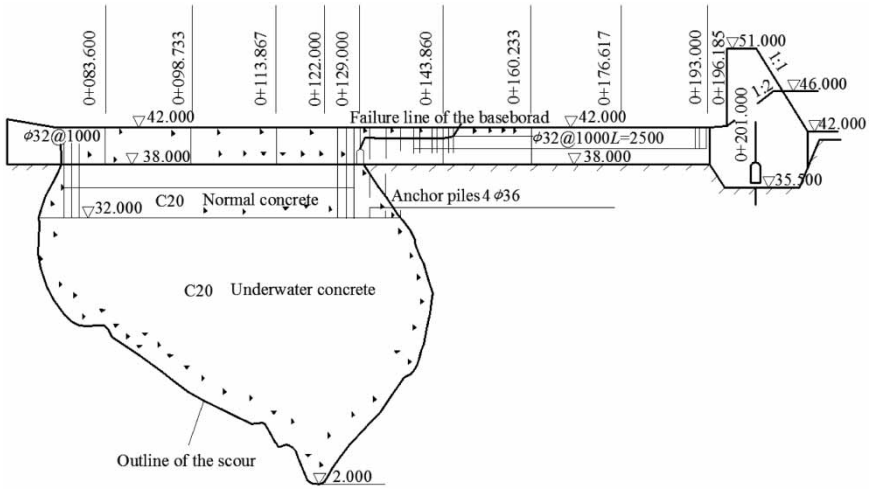

Figure 13 | The scour pit appeared in the right stilling pool.

of the rock bed is 1.6. A numerical model was established to reproduce the flow regime under the conditions where the right stilling basin was damaged. Because the No. 2 orifice was fully open with the largest unit discharge of 279 m^2/s, a scour pit certainly appeared along the midline of the No. 2 orifice. Figure 14 shows the velocity vector diagram of the middle section of the No. 2 orifice, and the region of large horizontal velocity (0 + 082.000 to 0 + 127.000) correlates well with the region where the scour depth actually

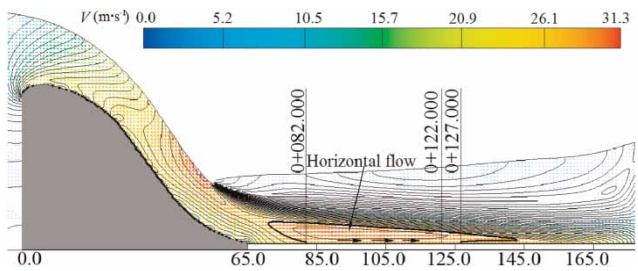

Figure 14 | Velocity vector diagram of the middle section of the No. 2 orifice.

Table 5 | Observed and predicted maximum scour depths for the Wuqiangxi Hydropower Station

	Predicted values			
Observed value	Proposed formula	Chen's formula	Martins' formula	Veronese formula
36.00 m	35.44 m	28.93 m	39.10 m	68.61 m
Absolute deviation	0.56 m	7.07 m	3.1 m	32.61 m
Relative error	1.56%	19.64%	8.61%	90.58%

happened ($0+082.000$ to $0+129.000$), as shown in Figure 13. The maximum velocity, V_m, at steady-state conditions near the flat bed is 31.3 m/s and located at $0+122.000$ m. Table 5 shows the observed and predicted maximum scour depths for the Wuqiangxi Hydropower Station. With the proposed model, the maximum scour depth is 35.44 m, and the absolute deviation between the predicted and the measured (36.0 m) values for the maximum scour depth is 0.56 m. The relative error of this deviation is 1.56%. However, the result is 28.93 m using Chen's formula, with an absolute deviation of 7.07 m and a relative error of 19.64%; 39.10 m by Martins' formula with an absolute deviation of 3.1 m and a relative error of 8.61%; and 68.61 m by the Veronese formula with an absolute deviation of 32.61 m and a relative error of 90.58%. The results obtained show that the proposed formula based on CFD (i.e. Equation (12)), can effectively estimate the maximum scour depth on a rocky bed downstream of overflow dams.

CONCLUSIONS

In this paper, a new formula for predicting the maximum scour depth of the rock bed downstream of overflow dams has been proposed based on the CFD technique. The three-dimensional flow field of overflow dams was simulated using the Flow-3D software. The results of the hydraulic model test of a practical project were compared with the results of the numerical model for verification. A power-law relationship between the output of the numerically simulated flow field over a flat rock bed and the observed scour depth was established and regressed using the LM algorithm. The proposed formula can effectively predict the maximum scour depth, and the results of this formula were verified by comparisons with the results of the three other formulae. Finally, applying the method to Wuqiangxi Hydropower Station provided a satisfactory result that is consistent with the actual conditions.

The numerical methodology is capable of reasonably predicting the flow field of spillway flows provided that the disposal approach, including the mesh resolutions, turbulence options, boundary conditions and numerical options is reasonable. The FAVOR method was applied to define the complex geometry, and the free surface was computed using the VOF method. The finite-volume method was used to solve the RANS equations, and RNG models were employed as turbulence closure models. The procedure for reducing the mesh size was completed, and a 0.1 m mesh was selected owing to the high accuracy achieved with less computational time. The comparison of the measured and simulated results shows that the CFD method can effectively simulate the flow field and the velocity distraction of overflow dams.

A power-law model for predicting the maximum scour depth, which was fitted using 18 sets of data and tested on 6 sets of data, has a small RMSE of 2.02 and a high CC of 0.9852. The comparison of the proposed formula and the three other formulae indicates that the proposed formula based on CFD can effectively estimate the ultimate scour depth. The maximum scour depth of the Wuqiangxi project was estimated with the proposed formula, and the absolute deviation between the predicted and the measured values (36.0 m) for the maximum scour depth is 0.56 m. The relative error of this deviation is 1.56%.

In the future, the air entrainment model used in Flow-3D and the application of this model to the prediction of plunge pool scour should be verified and discussed. Second, more practical cases of erosion damage downstream of overflow dams should be collected, and the maximum axial length and width of the scour hole need to be studied. Third, the experimental test results provided by Kunming hydropower investigation, Design & Research Institute, HECC, were used provisionally for the verification of the numerical model. In the future, when the complete published data are available, the numerical model should be verified using the new data. Moreover, a composite and simple scour coefficient of bedrock, K, was applied to represent the complicated erosion

resistance of the rock bed in this study, and a more advanced method which can simulate the actual rock properties should be developed in future research. Finally, the object of this study was maximum scour depth, which is not related to time evolution, so scouring process with time should be studied in the future.

ACKNOWLEDGEMENTS

The authors gratefully acknowledge the support of the State Key Laboratory of Hydraulic Engineering Simulation and Safety (Tianjin University), the Foundation for Innovative Research Groups of the National Natural Science Foundation of China (grant no. 51021004) and Tianjin Research Program of Application Foundation and Advanced Technology (grant no. 13JCYBJC19400). In addition, the authors would also like to thank Kunming Hydropower Investigation, Design & Research Institute, HECC, for their invaluable experimental test results.

REFERENCES

Azamathulla, H. M. 2013 Comments on 'Evaluation of selected equations for predicting scour at downstream of ski-jump spillway using laboratory and field data' by Chandan Kumar, P. Sreeja. *Eng. Geol.* **152** (1), 210–211.

Azamathulla, H. M., Deo, M. C. & Deolalikar, P. B. 2008a Alternative neural networks to estimate the scour below spillways. *Adv. Eng. Softw.* **39** (8), 689–698.

Azamathulla, H. M., Ghani, A. A., Zakaria, N. A., Lai, S. H., Chang, C. K., Leow, C. S. & Abuhasan, Z. 2008b Genetic programming to predict ski-jump bucket spillway scour. *J. Hydrodyn.* **20** (4), 477–484.

Azamathulla, H. M. 2006 Neural Networks to Estimate Scour Downstream of Ski-jump Bucket Spillway. *PhD Thesis*, Indian Institute of Technology, Bombay.

Azamathulla, H. M., Deo, M. C. & Deolalikar, P. B. 2005 Neural networks for estimation of scour downstream of a ski-jump bucket. *J. Hydraul. Eng.* **131** (10), 898–908.

Azamathulla, H. M., Deo, M. C. & Deolalikar, P. B. 2006 Estimation of scour below spillways using neural networks. *J. Hydraul. Res.* **44** (1), 61–69.

Beltaos, S. & Rajaratnam, N. 1973 Plane turbulent impinging jets. *J. Hydraul. Res.* **11** (1), 29–59.

Bey, A., Faruque, M. A. & Balachandar, R. 2007 Two-dimensional scour hole problem: Role of fluid structures. *J. Hydraul. Eng.* **133** (4), 414–430.

Bollaert, E. & Schleiss, A. 2003 Scour of rock due to the impact of plunging high velocity jets Part I: a state-of-the-art review. *J. Hydraul. Res.* **41** (5), 451–464.

Bollaert, E. & Schleiss, A. 2005 Physically based model for evaluation of rock scour due to high-velocity jet impact. *J. Hydraul. Eng.* **131** (3), 153–165.

Bureau of Indian Standards (BIS) 1985 Criteria for hydraulic design of bucket type energy dissipators. BIS: 7365 (2nd revision).

Canepa, S. & Hager, W. H. 2003 Effect of jet air content on plunge pool scour. *J. Hydraul. Eng.* **129** (5), 358–365.

Chen, C. T. 1963 An estimating formula for the local scour depth for the sky-jump energy dissipation. *J. Hydraul. Eng.* **2**, 13–23 (in Chinese).

D'Agostino, V. & Ferro, V. 2003 Scour on alluvial bed downstream of grade-control structures. *J. Hydraul. Eng.* **130** (1), 24–37.

Deng, J., Xu, W. L., Qu, J. X. & Yang, Y. Q. 2002 Analysis of rocky beds scouring characteristics. *J. Sichuan Univ. (Engineering Science Edition)* **34** (6), 32–35 (in Chinese).

Dey, S. & Sarkar, A. 2006 Scour downstream of an apron due to submerged horizontal jets. *J. Hydraul. Eng.* **132** (3), 246–257.

Ge, L., Lee, S. O., Sotiropoulos, F. & Sturm, T. 2005 3D unsteady RANS modeling of complex hydraulic engineering flows II: Model validation and flow physics. *J. Hydraul. Eng.* **131** (9), 809–820.

Ghodsian, M., Mehraein, M. & Ranjbar, H. R. 2012 Local scour due to free fall jets in non-uniform sediment. *Sci. Iranica A* **19** (6), 1437–1444.

Guan, H., Chen, W. R., Huang, N. & Yang, H. J. 2010 Estimation of reliability and cost relationship for architecture-based software. *Int. J. Automat. Comp.* **7** (4), 603–610.

Guven, A. & Azamathulla, H. M. d. 2012 Gene-expression programming for flip bucket spillway scour. *Water Sci. Technol.* **65** (11), 1982–1987.

Haltigin, T. W., Biron, P. M. & Lapointe, M. F. 2007 Predicting equilibrium scour-hole geometry near angled stream deflectors using a three-dimensional numerical flow model. *J. Hydraul. Eng.* **133** (8), 983–988.

Hirt, C. W. & Sicilian, J. M. 1985 A porosity technique for the definition of obstacles in rectangular cell meshes. In: *Proc. Fourth International Conf. Ship Hydro*, Washington, DC, pp. 1–19.

Huai, W. X., Wang, Z. W., Qian, Z. D. & Han, Y. Q. 2011 Numerical simulation of sandy bed erosion by 2D vertical jet. *Sci. China Technol. Sci.* **54** (12), 3265–3274.

Johnson, M. C. & Savage, B. M. 2006 Physical and numerical comparison of flow over ogee spillway in the presence of tailwater. *J. Hydraul. Eng.* **132** (12), 1353–1357.

Li, A. H. & Liu, P. Q. 2010 Mechanism of rock-bed scour due to impinging jet. *J. Hydraul. Res.* **48** (1), 14–22.

Lian, J. J. & Yang, M. 2008 *Hydrodynamics for High Dam*. China Water Conservancy and Hydropower Press, Beijing.

Liu, P. Q. 1994 Mechanism of Free Jet's Scour on Rocky River-Beds, Dissertation, Tsinghua University.

Liu, P. Q. 2005 A new method for calculating depth of scour pit caused by overflow water jets. *J. Hydraul. Res.* **43** (6), 696–702.

Liu, X. & Garciá, M. H. 2006 Numerical simulation of local scour with free surface and automatic mesh deformation. In: *Proceedings of World Environmental and Water Resource Congress*, Omaha, NE.

Liu, P. Q. & Li, A. H. 2007 Fluctuating uplift acting on rock blocks at the bottom of river bed and estimation of the limiting scour depth. *J. Hydraul. Res.* **45** (4), 478–485.

Manso, P. A., Fiorotto, V., Bollaert, E. & Schleiss, A. J. 2004 Discussion of 'Effect of jet air content on plunge pool scour' by Stefano Canepa and Willi H. Hager. *J. Hydraul. Eng.* **130**, 1130–1131.

Oliveto, G., Comuniello, V. & Bulbule, T. 2011 Time-dependent local scour downstream of positive-step stilling basins. *J. Hydraul. Res.* **49** (1), 105–112.

Pagliara, S., Hager, W. H. & Minor, H. E. 2006 Hydraulics of plane plunge pool scour. *J. Hydraul. Eng.* **132** (5), 450–461.

Spurr, K. J. W. 1985 Energy approach to estimating scour downstream of a large dam. *Int. Water Power Dam Constr.* **37** (7), 81–89.

Standard of Ministry of Water Resources, PRC. 2005 *Design Specification for Concrete Gravity Dams (SL319–2005)*. China Water Power Press, Beijing.

Termini, D. & Sammartano, V. 2012 Morphodynamic processes downstream of man-made structural interventions: Experimental investigation of the role of turbulent flow structures in the prediction of scour downstream of a rigid bed. *Phys. Chem. Earth, A/B/C* **49**, 18–31.

Zhang, J. M., Chen, J. G., Xu, W. L., Wang, Y. R. & Li, G. J. 2011 Three-dimensional numerical simulation of aerated flows downstream sudden fall aerator expansion in a tunnel. *J. Hydrodyn., Ser. B* **23** (1), 71–80.

First received 20 September 2013; accepted in revised form 5 April 2014. Available online 23 April 2014